Magnetoelectric responses induced by domain rearrangement and spin structural change in triangular-lattice helimagnets NiI_2 and CoI_2

T. Kurumaji,[1] S. Seki,[1] S. Ishiwata,[1] H. Murakawa,[2] Y. Kaneko,[2,3] and Y. Tokura[1,2,3]

[1]*Department of Applied Physics, University of Tokyo, Tokyo 113-8656, Japan*

[2]*Cross-Correlated Materials Research Group (CMRG) and Correlated Electron Research Group (CERG), RIKEN Advanced Science Institute, Wako 351-0198, Japan*

[3]*Multiferroics Project, ERATO, Japan Science and Technology Agency (JST), Tokyo 113-8656*

(Received 23 September 2012; published 25 January 2013)

Dielectric and magnetic properties have been investigated for single crystals of triangular-lattice antiferromagnets NiI_2 and CoI_2. For NiI_2, the proper screw spin order with the magnetic modulation vector $q \sim (0.138,0,1.457)$ induces electric polarization (P) along the in-plane direction with respect to the triangular lattice basal plane. The P shows monotonic increase as a function of the poling magnetic field (H) along the in-plane direction, suggesting the H-induced rearrangement of the multiferroic domain out of six possible domains. For CoI_2, both in-plane and out-of-plane components of P emerge in the helimagnetic ground state, in which two cycloidal magnetic phases with $q_1 = (\frac{1}{12}, \frac{1}{12}, \frac{1}{2})$ and $q_2 = (\frac{1}{8}, 0, \frac{1}{2})$ are supposed to coexist. The application of the in-plane H induces two-step metamagneticlike transitions, which probably goes through another ferroelectric helimagnetic phase as well as a paraelectric spin-collinear phase. Such distinctive magnetoelectric responses in the two simple triangular lattice antiferromagnets demonstrate that even a slight difference in the balance of magnetic interactions leads to a dramatic change of resultant magnetoelectric response in frustrated magnets.

DOI: 10.1103/PhysRevB.87.014429 PACS number(s): 75.85.+t, 77.80.Fm, 75.45.+j

I. INTRODUCTION

Magnetoelectric (ME) effects, i.e., magnetic (electric) control of dielectric (magnetic) properties, have been studied extensively from the viewpoint of both fundamental physics and potential application to spintronics.[1] A possible strategy to obtain a large ME effect is the employment of multiferroics, i.e., materials with both magnetic and dielectric orders.[2] However, such multiferroics turned out to be rather rare and the coupling between these orders is very weak in general. One recent breakthrough is the discovery of magnetically-induced ferroelectricity in several frustrated magnets, where helical spin texture induces electric polarization.[3] Because of strong coupling between spin texture and electric polarization (P), giant ME responses such as reversal, flop, and rotation of P by external magnetic field (H) can be obtained.[4] So far, the most successful microscopic model to explain the magnetically induced P in helimagnets is the inverse Dzyaloshinskii-Moriya (D-M) model,[5,6] which originates from relativistic spin-orbit interaction. This model predicts local electric polarization $\boldsymbol{p}_{ij}$ induced between two neighboring spins $\boldsymbol{S}_i$ and $\boldsymbol{S}_j$ in the form of $\boldsymbol{p}_{ij} \propto \boldsymbol{e}_{ij} \times (\boldsymbol{S}_i \times \boldsymbol{S}_j)$, where $\boldsymbol{e}_{ij}$ is the unit vector connecting the neighboring spins. This mechanism successfully explains the ferroelectricity and ME natures in several cycloidal helimagnets such as $R\mathrm{MnO_3}$,[7,8] $Ni_3V_2O_8$,[9] and $MnWO_4$,[10] in which the spins rotate within the plane including the magnetic modulation vector q.

In contrast, still yet to be clarified is the magnetoelectric coupling in triangular lattice antiferromagnets, one of the most typical and simplest examples of frustrated spin systems. When only the nearest neighbor exchange interaction is considered, the neighboring classical spins on triangular lattice make an angle of 120° with respect to each other. While the inverse D-M scheme predicts $P = 0$ for such a 120° spin texture, the appearance of nonzero P has recently been reported for yavapaiite $RbFe(MoO_4)_2$[11] and delafossite $CuCrO_2$.[12–14] The further introduction of next nearest and interplane interactions as well as magnetic anisotropy leads to the formation of more versatile spin textures. For example, delafossite $CuFe_{1-x}Ga_xO_2$ shows proper screw spin texture, where spins rotate within a plane normal to magnetic modulation vector $q \parallel \langle 110 \rangle$.[15,16] Whereas the inverse D-M model denies the ferroelectricity in such a proper screw spin state, emergence of $P \parallel q$ has recently been reported for $CuFe_{1-x}Ga_xO_2$. The origin of spin-driven ferroelectricity in the above delafossite compounds has been ascribed to the recently proposed mechanism of spin-dependent metal-ligand hybridization[17–19] which also stems from spin-orbit interaction to give rise to the local electric polarization in the form of $\boldsymbol{p}_{ij} \propto (\boldsymbol{e}_{ij} \cdot \boldsymbol{S}_i)\boldsymbol{S}_i - (\boldsymbol{e}_{ij} \cdot \boldsymbol{S}_j)\boldsymbol{S}_j$. Nevertheless, the general relationship between spin texture and electric polarization on a triangular lattice still remains elusive.

Our target materials, transition metal dihalides MX_2 (M: transition metal, X: halogen), have long been studied as one of the prototypes of antiferromagnets with a triangular lattice.[20,21] While early studies focus on their magnetic and optical properties, recent discovery of the coupling between helimagnetism and ferroelectricity in triangular lattice antiferromagnets MnI_2[22] and $NiBr_2$[23] as well as Jahn-Teller distorted $CuCl_2$[24] and $CuBr_2$[25] highlight MX_2 as the first example of multiferroic halides. In this paper, we investigate magnetic and dielectric properties of triangular lattice helimagnets NiI_2 and CoI_2, as characterized by the proper screw and cycloidal spin texture, respectively. We found that both compounds show ferroelectricity at their helimagnetic ground states. The H-induced rearrangement of helimagnetic domains is observed for NiI_2, while the H-induced transition into another helimagnetic phase is observed for CoI_2. Each phenomenon leads to a unique response of P under external H despite the similarity in the original crystal lattice, thereby indicating

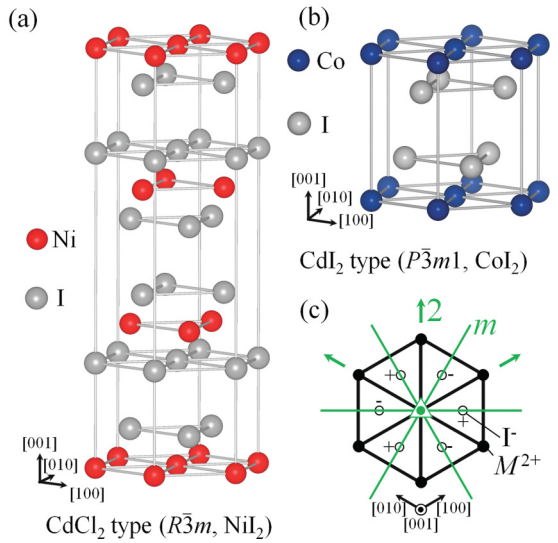

FIG. 1. (Color online) The crystallographic unit cell of (a) $CdCl_2$ type and (b) CdI_2 type structure. (c) The (001) projection of a triangular-lattice layer of M^{2+} ions (filled circles) and two adjacent I^- layers (open circles). Plus (minus) signs indicate that the position of the I atoms is above (below) the M^{2+} layer. The symmetry elements at an M^{2+} site are also indicated: reflection mirrors (m), twofold rotation axes (2), and a threefold rotation axis along the [001] axis with an inversion center (a triangle with a small circle).

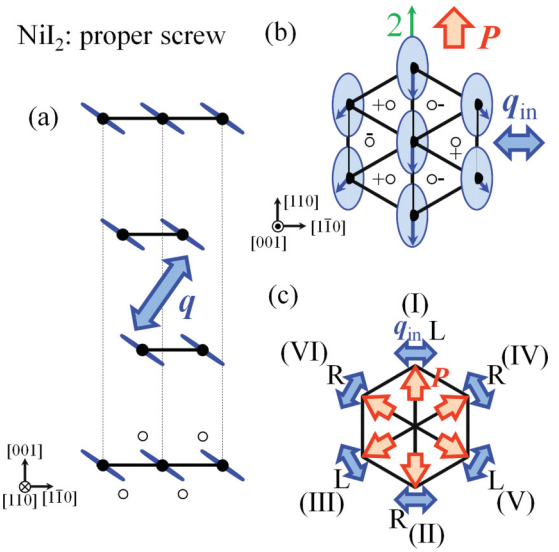

FIG. 2. (Color online) (a) and (b) Schematic illustration of the proper screw spin order with the magnetic modulation vector $q \sim (0.138,0,1.457)$ reported for NiI_2, viewed from the (a) [110] direction or (b) [001] direction. Blue bars in (a) indicate the spin-spiral plane. The compatible symmetry element as well as the allowed electric polarization (P) direction is indicated in (b). Closed (open) circles indicate Ni (I) atoms. (c) Six possible multiferroic domains with $P \parallel \langle 110 \rangle$, (I)~(VI). Corresponding in-plane magnetic modulation vector q_{in} and spin chirality (denoted as R or L) are also indicated.

that even a slight difference in the magnetic interactions is critically reflected in the respective magnetoelectric response in frustrated magnets.

II. STRUCTURAL AND MAGNETIC PROPERTIES

Most of transition metal dihalides MX_2 with X = Cl, Br, and I crystallize into a CdI_2 type ($P\bar{3}m1$) or $CdCl_2$ type ($R\bar{3}m$) structure, where each element forms a triangular lattice and stacks along the [001] axis in the sequence of $-(XMX)-(XMX)-$. The difference between these two structures is in the stacking pattern of (XMX) blocks; the $CdCl_2$ type structure is of the rhombohedral form with a repeating stack of three (XMX) layers [Fig. 1(a)], while the CdI_2 type structure does the straight stacking [Fig. 1(b)]. The magnetic properties are dominated by M^{2+} ions, which are surrounded by the octahedron of X^-. Since each magnetic M layer is separated by two adjacent nonmagnetic X layers, these compounds can be considered as a quasi-two-dimensional spin system.

NiI_2 crystallizes into the $CdCl_2$ type structure [Fig. 1(a)] with a magnetic Ni^{2+} ion ($S = 1$), and undergoes two successive antiferromagnetic phase transitions at $T_{N1} = 76$ K, and $T_{N2} = 59.5$ K[26–28] under zero magnetic field. The proper screw magnetic structure is realized at the magnetic ground state below T_{N2}, where spins rotate within the plane perpendicular to the magnetic modulation vector $q \sim (0.138,0,1.457)$. This means that the q vector is slanted off from the triangular-lattice basal plane. Correspondingly, the spin-spiral plane is also canted from the plane including the [001] axis [Fig. 2(a)]. For simplicity, hereafter, we define q_{in} as the in-plane component of the q vector [Fig. 2(b)].

In contrast, CoI_2 crystallizes into the CdI_2 type structure [Fig. 1(b)]. Magnetism is determined by Co^{2+}, which is in the high spin configuration ($t_{2g}^5 e_g^2$).[29–32] The spins are confined in the (001) plane due to the easy-plane anisotropy, which is confirmed by magnetization measurements and the Mössbauer spectroscopy.[28,33] A previous powder neutron diffraction study[28] suggested the emergence of cycloidal spin order with commensurate magnetic modulation vector $q = (\frac{1}{8},0,\frac{1}{2})$ below 8 K, where the spin spiral plane lies in the triangular-lattice plane [Fig. 7(g)]. On the other hand, the subsequent single crystal neutron diffraction study[34] reported that CoI_2 undergoes successive magnetic phase transitions at $T_{N1} = 11$ K and $T_{N2} = 9.4$ K while keeping two magnetic reflections at $q_1 = (\frac{1}{12},\frac{1}{12},\frac{1}{2})$ and $q_2 = (\frac{1}{8},0,\frac{1}{2})$ below T_{N1}. This suggests the presence of a multiple-q state or coexistence of two different single-q states, although the details are still yet to be clarified.

III. EXPERIMENTAL DETAILS

Single crystals of NiI_2 and CoI_2 were grown by the Bridgman method. Because of their moisture sensitivity, the handling of the sample was mostly performed in a glove box filled with Ar gas. The typical dimension of the crystal is 5 mm × 5 mm × 5 mm for NiI_2 and 3 mm × 3 mm × 1 mm for CoI_2. They were cleaved along the (001) plane, and cut into a rectangular shape with additional faces perpendicular to the (001) plane. The in-plane crystal orientation was determined by the x-ray Laue method for NiI_2, but not for CoI_2 due to high instability of the sample in the air. Silver paste was painted on the selected surfaces as the electrodes.

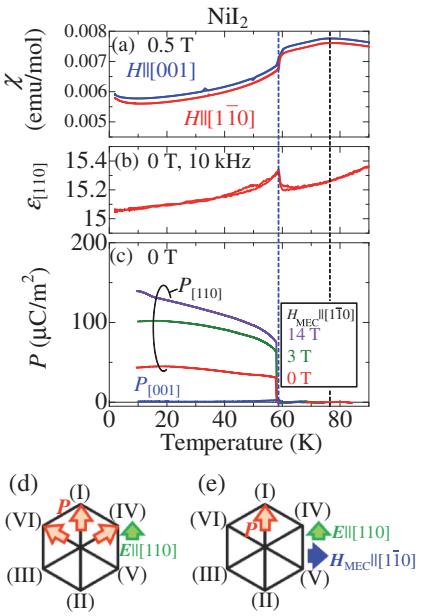

FIG. 3. (Color online) (a)–(c) The temperature dependence of magnetic susceptibility χ, the [110] component of ε ($\varepsilon_{[110]}$), and electric polarization P measured for NiI_2. The [110] component of P ($P_{[110]}$) was measured in the warming process without E and H after the field cooling with $E \parallel [110]$ and $H \parallel [1\bar{1}0]$ (denoted as H_{MEC}). (d) and (e) Favorable domain distribution under the electric field (E) and the magnetic field (H_{MEC}).

The P value was deduced by the time integration of the polarization current measured by an electrometer with constant rates of temperature (T) sweep ($1\sim 5$ K/min). To enlarge the population of a specific P domain, the poling electric field ($E = 70 \sim 120$ kV/m) was applied in the cooling process and removed just prior to the measurements of polarization current in the warming process. Unless specified, the H was kept unchanged during both procedures. Dielectric constant ε was measured at 10–100 kHz using an LCR meter. M was measured with a SQUID magnetometer.

IV. RESULTS AND DISCUSSION

A. NiI_2

First, we investigate the magnetic and dielectric nature of NiI_2 at the magnetic ground state around $H = 0$. Figures 3(a)–3(c) show the T dependence of magnetic susceptibility $\chi(= M/H)$, the [110] component of dielectric constant ε ($\varepsilon_{[110]}$), and [110] and [001] components of electric polarization P ($P_{[110]}$ and $P_{[001]}$). χ shows a broad peak at $T_{N1} \sim 76$ K and a sudden drop at $T_{N2} \sim 58$ K both for $H \parallel [1\bar{1}0]$ and $H \parallel [001]$, which are consistent with the previous reports.[28] The latter anomaly signals the onset of the proper screw spin order with $q_{in} \parallel \langle 1\bar{1}0 \rangle$. Simultaneously, the $\varepsilon_{[110]}$ shows a peak and $P_{[110]}$ begins to develop. The sign of P can be reversed with an opposite direction of poling E, and no dielectric anomaly is detected along the [001] direction. These results suggest that the proper screw magnetic ground state induces ferroelectric polarization along the in-plane direction, while the intermediate magnetic state between T_{N1} and T_{N2} is paraelectric in nature. This behavior can be justified from the viewpoint of symmetry. In the case of NiI_2, the original crystal structure possesses centrosymmetric site symmetry $\bar{3}m$ at magnetic Ni sites [Fig. 1(c)]. The proper screw magnetic order with $q_{in} \parallel \langle 1\bar{1}0 \rangle$ breaks several symmetry elements including the inversion center, and only the twofold rotation axis perpendicular to both the q_{in} vector and the [001] axis remains unbroken. Thus, the emergence of $P \parallel [110] (\perp q_{in})$ can be allowed [Fig. 2(b)]. The inverse D-M model predicts $P = 0$ for the *simple* proper screw magnetic order where the q vector is along the high-symmetry axis (e.g., [110] or $[1\bar{1}0]$). However, given that the interlayer coupling is much weaker than the intralayer coupling, the inverse D-M mechanism can be the

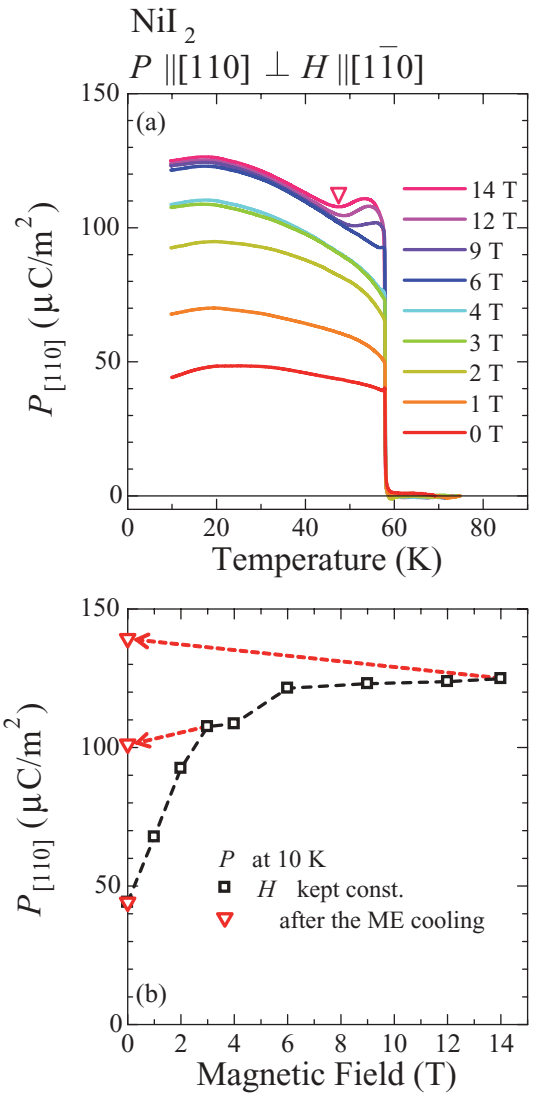

FIG. 4. (Color online) (a) The temperature dependence of $P_{[110]}$ measured for NiI_2 under various magnitudes of H applied along the $[1\bar{1}0]$ axis. $P_{[110]}$ was measured in the warming process without E after the field cooling with $E \parallel [110]$, while applied H was unchanged during both procedures. The small open triangle indicates the onset of the magnetically-induced hump structure in the P-T curve. (b) Magnetic field dependence of $P_{[110]}$ value at 10 K, obtained from the P-T scans in Fig. 4(a) (open squares) and Fig. 3(c) (triangles). The data points taken with the same magnitude of poling magnetic field H_{MEC} (=3 T or 14 T) are connected by dashed arrows.

origin of nonzero $P_{[110]}$ due to the canting of the spin spiral plane towards the triangular-lattice plane. On the other hand, the metal-ligand hybridization model may also be relevant to the observed ferroelectricity of magnetic origin. Similar coupling between in-plane P and proper screw spin order with $q_{\rm in} \parallel \langle 1\bar{1}0 \rangle$ has recently been reported for a triangular lattice helimagnet MnI_2.[22]

Next, we discuss the effect of magnetic field cooling. Figure 3(c) summarizes the temperature dependence of $P_{[110]}$ in the warming run, measured without E and H after the field-cooling procedures with $E \parallel [110]$ and various magnitudes of $H \parallel [1\bar{1}0]$ ($H_{\rm MEC}$, the suffix MEC standing for magneto-electric cooling). We found that $P_{[110]}$ becomes larger as the magnitude of $H_{\rm MEC}$ increases. This behavior probably originates from the H-induced rearrangement of multiferroic domains as discussed below. In general, the transition from paramagnetic to magnetically ordered state generates multiple domains, which can be converted into each other by the symmetry element that is broken by magnetic order.[35] Due to the symmetry of triangular lattice, NiI_2 can host six helimagnetic domains characterized by the unique set of three possible $q_{\rm in} \parallel \langle 1\bar{1}0 \rangle$ and two spin-chiral (helical sense) degrees of freedom, which have the one-by-one correspondence to the six ferroelectric domains with $P \parallel \langle 110 \rangle \perp q_{\rm in}$. In Fig. 2(c), the relationship among $q_{\rm in}$ direction, vector spin chirality, and P direction for each multiferroic domain is summarized. Note that the reversal of spin chirality always gives the opposite direction of P. When the specimen is cooled only with the poling $E \parallel [110]$, the ferroelectric domains with polarization component parallel to E [(I), (IV), and (VI) in Fig. 3(d)] should be selected. Thus, the finite $P_{[110]}$ is observed in the P-T scan with $H_{\rm MEC} = 0$ T [Fig. 3(c)]. On the other hand, the in-plane H should favor the domain with $P \perp q_{\rm in} \parallel H$ in the present case of the proper screw magnetic order with $q_{\rm in} \parallel \langle 1\bar{1}0 \rangle$, since antiferromagnetically aligned spins prefer to lie within a plane perpendicular to the applied H. When the specimen is cooled with both $E \parallel [110]$ and $H_{\rm MEC} \parallel [1\bar{1}0]$, the domain-(I) is dominantly generated [Fig. 3(e)]. By comparing Figs. 3(d) and 3(e), the enhancement of $P_{[110]}$ as a function of $H_{\rm MEC} \parallel [1\bar{1}0]$ can be reasonably explained in this way.

Figure 4(a) shows the T dependence of $P_{[110]}$ under various magnitudes of $H \parallel [1\bar{1}0]$. This time, $P_{[110]}$ was measured in the warming process without E after the cooling with $E \parallel [110]$, while the applied H was kept unchanged during both procedures. As H increases, the value of $P_{[110]}$ monotonically increases and saturates above $H = 6$ T. Figure 4(b) summarizes the H dependence of $P_{[110]}$ at 10 K (denoted as square symbols) deduced from the P-T profile in Fig. 4(a). In the same figure, also plotted are the $P_{[110]}$ values (triangles) at 10 K obtained from Fig. 3(c), i.e., measured at $H = 0$ after the field cooling with $H_{\rm MEC}$. For both 3 T and 14 T, the removal of external H after the field cooling (indicated with dashed

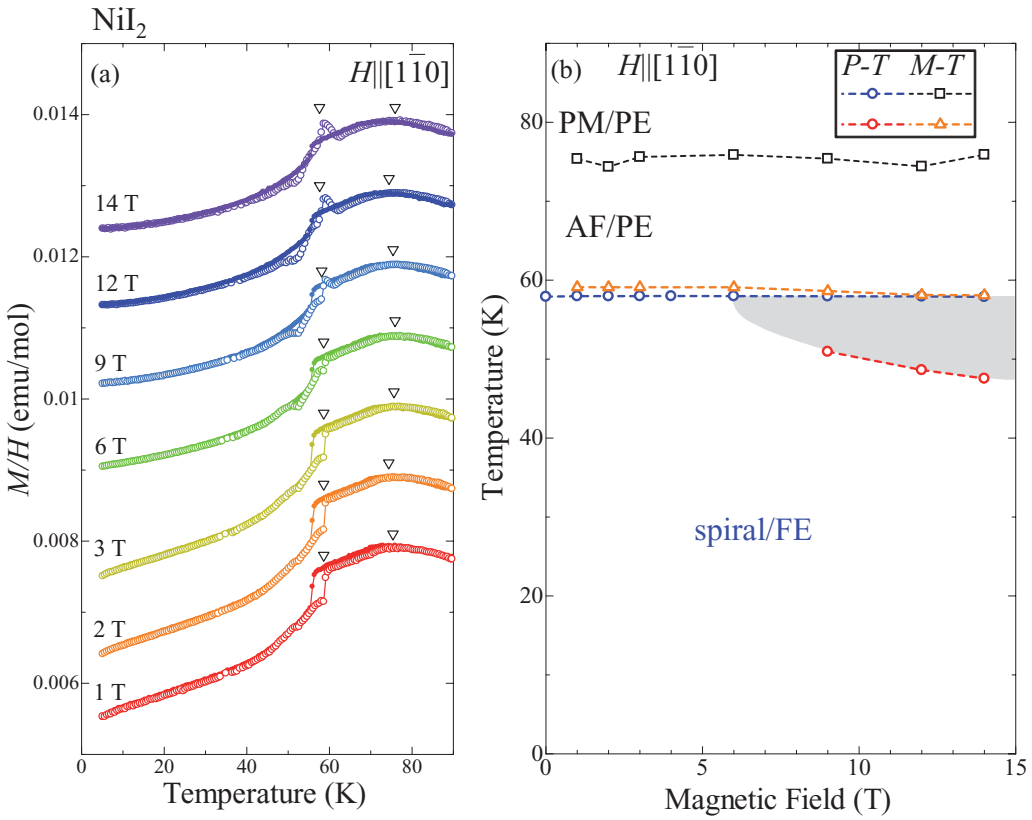

FIG. 5. (Color online) (a) The temperature dependence of M/H taken for NiI_2 under various magnitudes of $H \parallel [1\bar{1}0]$. The data (except for the one at 1 T) are arbitrarily offset for clarity. Solid (open) circles are data obtained in the cooling (warming) run. Open triangles indicate anomalies observed in the warming runs. The M/H profiles, except for the one with $H = 1$ T, are arbitrarily offset for clarity. (b) T-H phase diagram for NiI_2 with $H \parallel [1\bar{1}0]$, determined by various T scans of M and P.

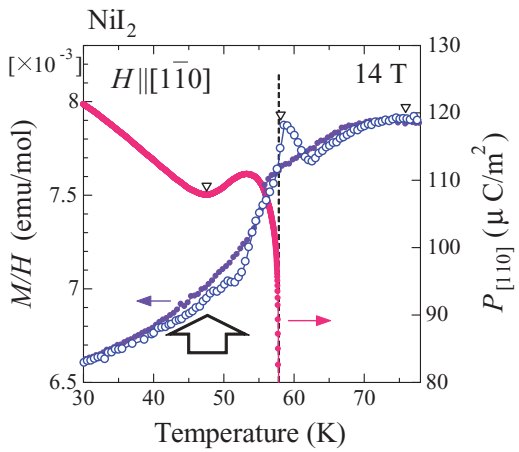

FIG. 6. (Color online) The temperature dependence of M/H and $P_{[110]}$ near the magnetic transition temperature at $H = 14$ T.

arrows) keeps the $P_{[110]}$ value almost constant, suggesting the observed H dependence of P originates from the domain rearrangement, not from the change in spin texture.

Figure 5(a) shows the T dependence of M/H $(=\chi)$ under various magnitudes of $H \parallel [1\bar{1}0]$. We found that the anomalies in M corresponding to T_{N1} and T_{N2} survive up to 14 T. In Fig. 5(b), the H-T phase diagram for $H \parallel [1\bar{1}0]$ determined from the various T and H scans of M and P is indicated. The boundary of the ferroelectric phase (FE) always coincides with that of the helimagnetic ground state, which proves the strong correlation between ferroelectricity and helimagnetism in this system. Note that with H higher than 9 T, the T dependence of $P_{[110]}$ is not monotonic, but has a hump structure slightly below the ferroelectric transition temperature [Fig. 4(a)]. In Fig. 6, the expanded view of T dependence of M/H and P at 14 T is indicated. We see the enhancement of $P_{[110]}$ for 47 K$< T <T_{N2} \sim 58$ K, where the M/H profile also shows noticeable anomalies with clear hysteresis. Since such behavior is not observed in the P-T scan performed at $H = 0$ after the magnetic field cooling [Fig. 3(c)], the observed nonmonotonous enhancement of P just below T_{N2} probably reflects the deformation of the magnetic structure under H. Such anomalies in the P-T profiles for various H values are also plotted in the H-T phase diagram [Fig. 5(b)], which implies the existence of another multiferroic phase in the high-H region (shaded area). In the case of triangular lattice helimagnet MnI_2 with the analogous spin texture,[36,37] the in-plane H induces a change of stable q_{in} direction from $q_{in} \parallel \langle 1\bar{1}0 \rangle$ to $q_{in} \parallel \langle 110 \rangle$ while keeping the proper screw spin structure.[22] A similar situation seems to occur for NiI_2, yet a further investigation of magnetic structure under H would be necessary to fully clarify the origin of observed magnetoelectric response.

B. CoI_2

Next, we investigate the magnetic and dielectric properties of triangular lattice helimagnet CoI_2. Figures 7(a)– 7(c) show the T dependence of χ, the in-plane component of ε (ε_{in}), and the in-plane and the out-of-plane component of P (P_{in} and $P_{[001]}$) measured for the magnetic ground state at $H \sim 0$. As T decreases, χ shows a sudden drop at $T_{N2} \sim 9$ K, signaling the onset of the helimagnetic ordering. Simultaneously, both P_{in} and $P_{[001]}$ begin to develop, while a possible anomaly in ε_{in} is too small to be detected. Since the ratio of $P_{[001]}$ to P_{in} is appreciable (∼0.3), the observed $P_{[001]}$ may not simply be ascribed to the leakage component of P_{in}. The sign of P can

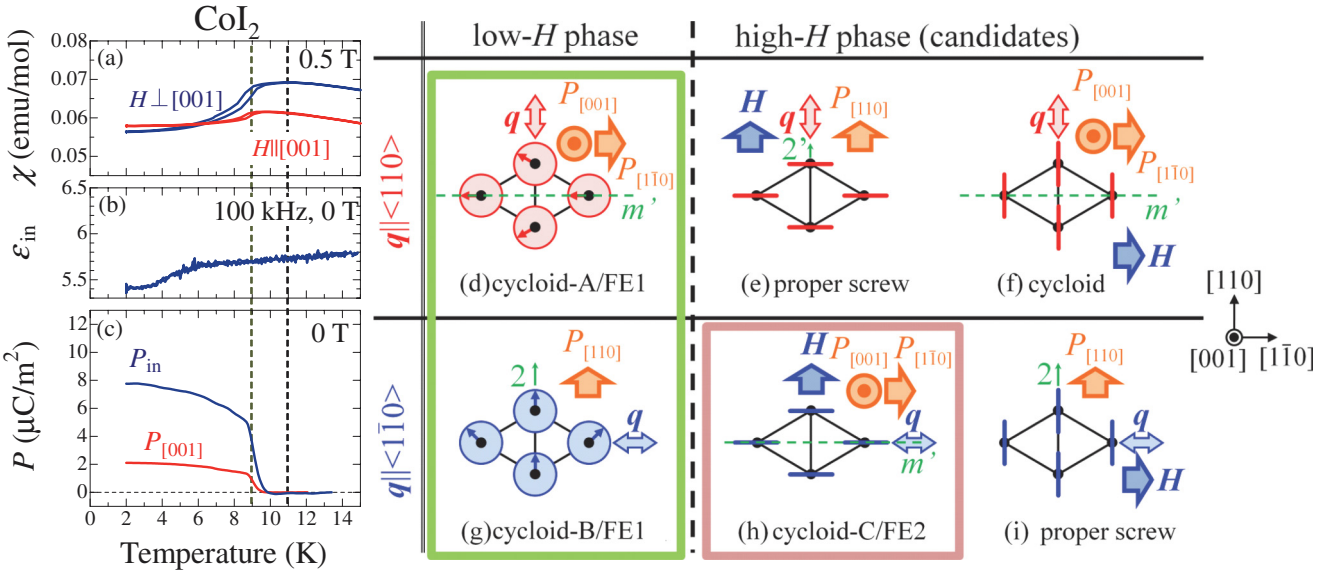

FIG. 7. (Color online) (a)–(c) The temperature dependence of χ, the in-plane component of ε (ε_{in}), and P for CoI_2. (d)–(i) Schematic illustrations of possible magnetic structures in CoI_2, viewed from the [001] direction. Upper (lower) row indicates the ones with $q \parallel \langle 110 \rangle$ ($q \parallel \langle 1\bar{1}0 \rangle$). In the magnetic ground state, the spin-spiral plane is confined within the (001) plane [(d) and (g)]. Application of in-plane H is expected to reorient the spin spiral into the $(1\bar{1}0)$ plane [(e) and (h)] or the (110) plane [(f) and (i)]. For each configuration, the compatible symmetry element and the possible electric polarization direction are indicated. Red or blue bars in (e), (f), (h), and (i) denote the spin spiral plane perpendicular to the (001) plane.

be reversed with an opposite direction of poling E. While the previous neutron diffraction study suggested the existence of the intervening spin-ordered state between $T_{N2} < T < T_{N1} \sim 11$ K, no corresponding magnetic or dielectric anomaly at T_{N1} can be detected in the current measurements. Our present results suggest that only the helimagnetic ground state hosts the ferroelectricity, and the intermediate phase is paraelectric in nature.

Following the result of a former neutron diffraction study,[28,34] we assume the coexistence of two cycloidal spin orders with $q \parallel \langle 110 \rangle$ or $q \parallel \langle 1\bar{1}0 \rangle$ to discuss the origin of induced P, as shown in Figs. 7(d) and 7(g). Both spin textures break most of the symmetry elements of the original crystal lattice characterized by the site symmetry $\bar{3}m$ at magnetic Co^{2+}site; the cycloidal order with $q \parallel \langle 110 \rangle$ leaves only the m' (mirror followed by time reversal) normal to q unbroken, and thus allows emergence of both $P_{[1\bar{1}0]}(\perp q)$ and $P_{[001]}$. In the cycloidal order with $q \parallel \langle 1\bar{1}0 \rangle$, on the other hand, only the in-plane two-fold rotation axis normal to q survives, therefore, and $P_{[110]}(\perp q)$ may appear. By considering the coexistence of these two kinds of spin textures, we can naturally explain the observed emergence of both the in-plane and the out-of-plane components of P in the helimagnetic ground state. In terms of the microscopic origin of ME coupling, the inverse D-M mechanism can predict only the in-plane component of P. By contrast, the metal-ligand hybridization scheme can be relevant to the appearance of $P_{[001]}$ as well. A similar situation has recently been reported for $NiBr_2$ which hosts cycloidal spin order with $q \parallel \langle 110 \rangle$.[23]

We further investigated the development of P and M under the in-plane H. Figure 8(a) shows the T dependence of M/H under various magnitudes of H applied perpendicular to the [001] axis. As H increases, T_{N2} (characterized by a sudden drop of M/H) gradually decreases and the transition at T_{N2} finally vanishes above 9 T. In Fig. 8(b), we plotted the corresponding profile of dM/dT (temperature derivative of M). Notably, in addition to the peak anomaly at T_{N2} (green triangles), we found another peak structure (red triangles) for the magnetic field range of $6\ \text{T} \leqslant H \leqslant 8$ T. Such a two-step metamagneticlike transition can also be identified in the H dependence of M below T_{N2} [Fig. 8(c)]; the H derivative of M (dM/dH) clearly shows the two peak structures [Fig. 8(d)] as in the case of the T scan. Based on various H and T scans of M, we have summarized the H-T magnetic phase diagram of CoI_2 under the in-plane H (Fig. 9). At the lowest temperature, at least three magnetic phases can be identified under the applied H up to 14 T. To elucidate the dielectric nature of each magnetic phase, we measured the T dependence of P_{in} under various magnitudes of in-plane H. Here, H is applied normal or parallel to the electrode, which corresponds to $P \perp H$ [Fig. 10(b)] or $P \parallel H$ [Fig. 10(d)] setup, respectively. For both conditions, the ferroelectric transition temperature decreases as H increases, and an additional anomaly in the P profile emerges for $6\ \text{T} \leqslant H \leqslant 8$ T. These phenomena can be identified from the double-peak structure in the pyroelectric current (I_p) profile [Figs. 10(a) and 10(c)], which corresponds to the T derivative of P. Such anomalies in P-T profiles are plotted in the H-T magnetic phase diagram as shown in Fig. 9. The magnetic anomalies always accompany the dielectric anomalies, confirming the strong magnetoelectric coupling in this system. Our measurements of P_{in} revealed

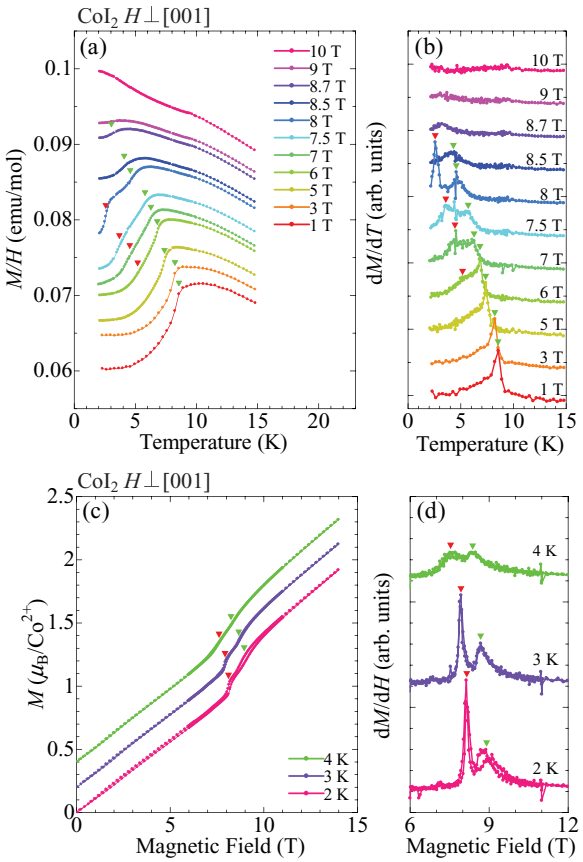

FIG. 8. (Color online) (a) The temperature dependence of M/H, measured for CoI_2 under various magnitudes of H applied perpendicular to the [001] axis. (b) The temperature derivative of magnetization dM/dT for the data taken in (a). (c) Magnetic field dependence of M measured with $H \perp [001]$ at various temperatures. (d) Magnetic field derivative of magnetization dM/dH for the data taken in (c). The triangles represent the transition points. In each figure, the data are arbitrarily offset for clarity, except for the ones taken at 1 T [(a) and (b)] or at 2 K [(c) and (d)].

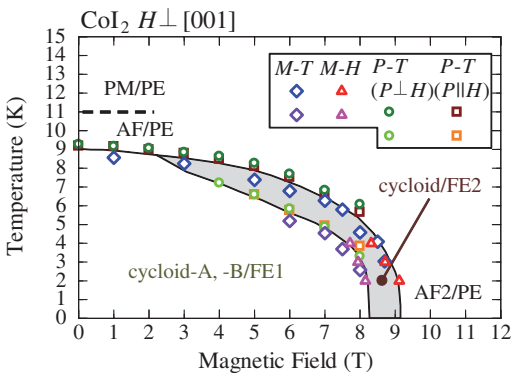

FIG. 9. (Color online) The T-H phase diagram for CoI_2 under H applied perpendicular to the [001] axis. The phase boundaries are determined by various T and H scans of M and P. The horizontal broken line represents the presumed phase boundary between paramagnetic (PM) and antiferromagnetic (AF) phases suggested by the neutron diffraction experiment in Ref. 34.

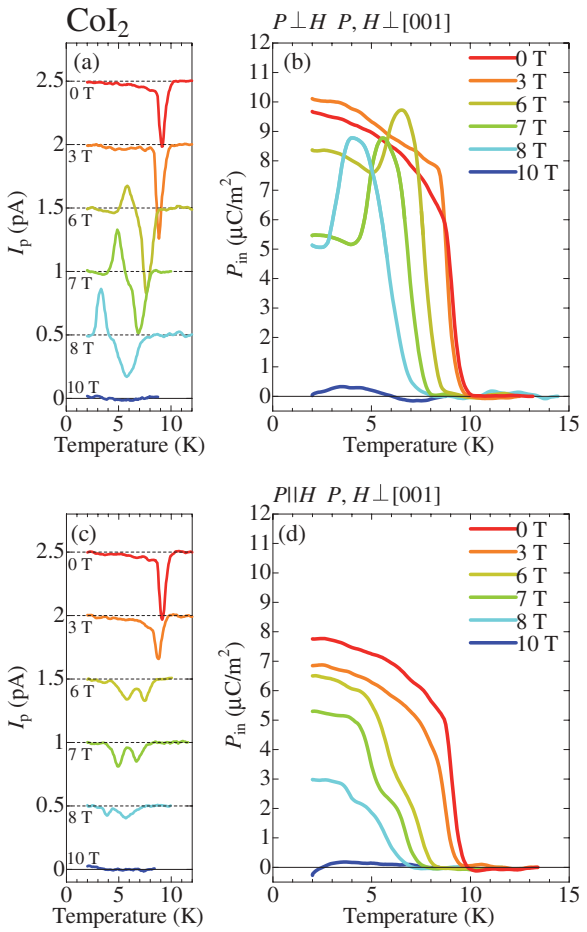

FIG. 10. (Color online) (a) The temperature dependence of the in-plane component of (a) pyroelectric current I_p and (b) electric polarization (P_{in}) measured for CoI_2 in the warming process without E, after the cooling with E. Here, the in-plane H is kept unchanged during both processes, which is applied normal to E. The corresponding data taken with the $E \parallel H$ poling condition is also shown in (c) and (d). In (a) and (c), the I_p-T profiles are arbitrarily offset for clarity, except for the ones at 10 T.

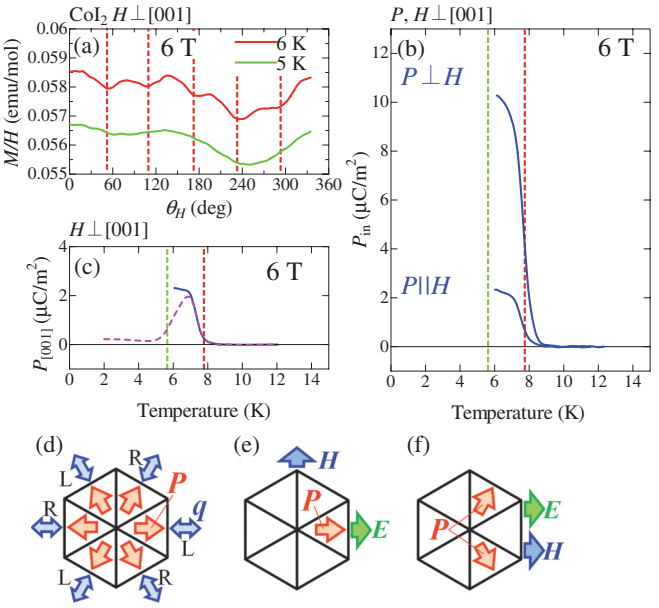

FIG. 11. (Color online) (a) The H-direction dependence of M/H measured at 6 T for CoI_2. Here, H is rotated around the [001] axis, and θ_H is defined as the angle between the H direction and an arbitrarily chosen in-plane crystallographic axis. (b) Temperature dependence of the in-plane component of P measured in the warming process without E, after the cooling down to 6 K with E. During both processes, in-plane H (applied parallel or normal to E) was kept unchanged. (c) Temperature dependence of the [001] component of P under the in-plane H. The solid (dashed) line represents the procedure that the specimen was cooled with the poling field of E from 15 K to 6 K (2 K); then E was switched off prior to the measurement in the T-increasing run. (d) Six possible multiferroic domains with unique in-plane P directions expected for the spin texture shown in Fig. 7(h). Corresponding in-plane magnetic modulation vector q_{in} and spin chirality (denoted as R or L) are indicated. Favorable domain distributions under various combinations of H and E are also indicated in (e) and (f).

that not only the helimagnetic ground state (FE1) but also the first H-induced magnetic phase (FE2: shadowed region) can induce electric polarization. P finally vanishes for the second H-induced magnetic phase (AF2), which may signal the collinear nature of spin arrangement in this H-T region.

In the following, we discuss the possible magnetic structure in the H-induced FE2 state. In general, the antiferromagnetic spins (or spin spiral plane) favor to lie normal to the external H. Thus, the application of in-plane H can cause the flop of the spin spiral from the triangular basal plane into the plane normal to H. To check the validity of the above scenario of spin flop, we measured the H-direction dependence of M/H at various T under $H = 6$ T [Fig. 11(a)]. Here, H is rotated around the [001] axis, and θ_H is defined as an angle between the H direction and the arbitrarily chosen in-plane crystallographic axis. We observed the oscillations of M/H with the cycle of 60° in the FE2 phase ($T = 6$ K), while not in the FE1 phase ($T = 5$ K). A similar oscillation of M/H with the cycle of 60° has recently been reported for the triangular-lattice spiral magnet $CuFe_{1-x}Ga_xO_2$,[38] where the rotation of the in-plane H causes the flop of the in-plane q so as to keep the spin-spiral plane normal to the external H. Note that this behavior is expected only when the spin spiral is normal (not parallel) to the triangular basal plane, since applied H cannot lift the degeneracy of in-plane q when the spin spiral lies in the (001) plane. The presently observed θ_H dependence of M/H suggests that the phase transition from FE1 (e.g., at 5 K and 6 T) into FE2 (e.g., at 6 K and 6 T) corresponds to the flop of the spin spiral plane from the (001) plane into the plane including the [001] axis.

In Figs. 7(e), 7(f), 7(h), and 7(i), we indicate the four possible spin-flopped states deduced from the cycloidal magnetic ground state with $q \parallel \langle 110 \rangle$ or $q \parallel \langle 1\bar{1}0 \rangle$. Based on the symmetry analysis as in the case of NiI_2 (see caption of Fig. 7), we can predict the relationship $P_{in} \parallel H$ for the $q \parallel \langle 110 \rangle$ state [Figs. 7(e) and 7(f)] and $P_{in} \perp H$ for the $q \parallel \langle 1\bar{1}0 \rangle$ state [Fig. 7(h) and 7(i)], respectively. Here, each spin texture can host six possible ferroelectric domains with unique in-plane P directions, and the application of E and H should enable the domain selection. As an example, in Figs. 11(d)–11(f), we show the expected correspondence among the six possible ferroelectric and helimagnetic domains

as well as the development of domain distribution under the external E and H for the spin texture shown in Fig. 7(h). To determine the plausible spin texture, we measured the T dependence of $P_{\rm in}$ in the FE2 state with the $P \perp H$ and $P \parallel H$ setup at 6 T [Fig. 11(b)]. Much larger $P_{\rm in}$ is observed in the $P \perp H$ setup than the $P \parallel H$ setup, implying that the $q \parallel \langle 1\bar{1}0 \rangle$ state favoring the $P_{\rm in} \perp H$ relationship is stabilized in the FE2 phase [Fig. 7(h) and 7(i)]. We further measured the T dependence of $P_{[001]}$ in the FE2 state at 6 T [Fig. 11(c)]. The symmetry analysis allows the emergence of nonzero $P_{[001]}$ at least for the spin texture shown in Fig. 7(h), which is consistent with experimental observation and hence plausible as the spin texture for the FE2 phase. To fully establish the H-induced development of the spin texture in the CoI_2, however, more detailed study including neutron diffraction experiments on single crystal is highly demanded.

V. CONCLUSION

In summary, we investigated magnetic and dielectric properties of single crystals of the triangular-lattice antiferromagnets NiI_2 and CoI_2. We found that both NiI_2 with screw spin order and CoI_2 with cycloidal spin order show spin-driven ferroelectricity in the helimagnetic ground state. In-plane H induces rearrangement of six possible multiferroic domains for NiI_2, and deformation of the helical spin texture for CoI_2, each of which causes unique and distinctive magnetoelectric response. In consideration of the structural similarities in these two triangular lattice systems, the spin ordering pattern as well as the resultant magnetoelectric behavior is determined on the delicate balance of magnetic interactions. Our present results demonstrate that even the simplest triangular lattice antiferromagnets can host a rich variety of multiferroic behaviors, which promises the further discovery of unique ME functions in frustrated magnets.

ACKNOWLEDGMENTS

This work was partly supported by Grant-in-Aids for Scientific Research (Grant Nos. 20340086 and 24224009) from the MEXT of Japan, and FIRST Program by JSPS.

[1] M. Fiebig, J. Phys. D **38**, R123 (2005).
[2] K. F. Wang, J.-M. Liu, and Z. F. Ren, Adv. Phys. **58**, 321 (2009).
[3] S.-W. Cheong and M. Mostovoy, Nat. Mater. **6**, 13 (2007).
[4] Y. Tokura and S. Seki, Adv. Mater. **22**, 1554 (2010).
[5] H. Katsura, N. Nagaosa, and A. V. Balatsky, Phys. Rev. Lett. **95**, 057205 (2005).
[6] I. A. Sergienko and E. Dagotto, Phys. Rev. B **73**, 094434 (2006).
[7] T. Kimura, T. Goto, H. Shintani, K. Ishizaka, T. Arima, and Y. Tokura, Nature (London) **426**, 55 (2003).
[8] T. Goto, T. Kimura, G. Lawes, A. P. Ramirez, and Y. Tokura, Phys. Rev. Lett. **92**, 257201 (2004).
[9] G. Lawes, A. B. Harris, T. Kimura, N. Rogado, R. J. Cava, A. Aharony, O. Entin-Wohlman, T. Yildrim, M. Kenzelmann, C. Broholm, and A. P. Ramirez, Phys. Rev. Lett. **95**, 087205 (2005).
[10] K. Taniguchi, N. Abe, T. Takenobu, Y. Iwasa, and T. Arima, Phys. Rev. Lett. **97**, 097203 (2006).
[11] M. Kenzelmann, G. Lawes, A. B. Harris, G. Gasparovic, C. Broholm, A. P. Ramirez, G. A. Jorge, M. Jaime, S. Park, Q. Huang, A. Y. Shapiro, and L. A. Demianets, Phys. Rev. Lett. **98**, 267205 (2007).
[12] S. Seki, Y. Onose, and Y. Tokura, Phys. Rev. Lett. **101**, 067204 (2008).
[13] K. Kimura, H. Nakamura, K. Ohgushi, and T. Kimura, Phys. Rev. B **78**, 140401 (2008).
[14] M. Soda, K. Kimura, T. Kimura, M. Matsuura, and K. Hirota, J. Phys. Soc. Jpn. **78**, 124703 (2009).
[15] T. Kimura, J. C. Lashley, and A. P. Ramirez, Phys. Rev. B **73**, 220401 (2006).
[16] T. Nakajima, S. Mitsuda, S. Kanetsuki, K. Tanaka, K. Fujii, N. Terada, M. Soda, M. Matsuura, and K. Hirota, Phys. Rev. B **77**, 052401 (2008).
[17] C. Jia, S. Onoda, N. Nagaosa, and J. H. Han, Phys. Rev. B **74**, 224444 (2006).
[18] C. Jia, S. Onoda, N. Nagaosa, and J. H. Han, Phys. Rev. B **76**, 144424 (2007).
[19] T. Arima, J. Phys. Soc. Jpn. **76**, 073702 (2007).
[20] A. Herpin, *Theorie du magnetisme* (Press Universitaires de France, Paris, 1968).
[21] K. Katsumata, M. Matsuura, and H. P. J. Wijn, *Magnetic Properties of Non-Metallic Inorganic Compounds Based on Transition Elements*, Landolt-Bërnstein, Group III: Condensed Matter, Vol. 27, Subvolume J1, Halides I (Springer-Verlag, Berlin, 1994), p. 4.
[22] T. Kurumaji, S. Seki, S. Ishiwata, H. Murakawa, Y. Tokunaga, Y. Kaneko, and Y. Tokura, Phys. Rev. Lett. **106**, 167206 (2011).
[23] Y. Tokunaga, D. Okuyama, T. Kurumaji, T. Arima, H. Nakao, Y. Murakami, Y. Taguchi, and Y. Tokura, Phys. Rev. B **84**, 060406 (2011).
[24] S. Seki, T. Kurumaji, S. Ishiwata, H. Matsui, H. Murakawa, Y. Tokunaga, Y. Kaneko, T. Hasegawa, and Y. Tokura, Phys. Rev. B **82**, 064424 (2010).
[25] L. Zhao, T.-L. Hung, C.-C. Li, Y.-Y. Chen, M.-K. Wu, R. K. Kremer, M. G. Banks, A. Simon, M.-H. Whangbo, C. Lee, J. S. Kim, I. Kim, and K. H. Kim, Adv. Mater. **24**, 2469 (2012).
[26] D. Billerey, C. Terrier, N. Ciret, and J. Kleinclauss, Phys. Lett. A **61**, 138 (1977).
[27] D. Billerey, C. Terrier, R. Mainard, and A. J. Pointon, Phys. Lett. A **77**, 59 (1980).
[28] S. R. Kuindersma, J. P. Sanchez, and C. Haas, Physica B **111**, 231 (1981).
[29] J. Ferguson, D. L. Wood, and K. Knox, J. Chem. Phys. **39**, 881 (1963).
[30] J. C. Christie, I. W. Johnstone, G. D. Jones, and K. Zdansky, Phys. Rev. B **12**, 4656 (1975).
[31] I. W. Johnstone and G. D. Jones, Phys. Rev. B **15**, 1297 (1977).
[32] S. R. Kuindersma, P. R. Boudewijn, and C. Haas, Phys. Status Solidi B **108**, 187 (1981).

[33]R. J. Pollard, V. H. McCann, and J. B. Ward, J. Phys. C **15**, 6807 (1982).
[34]M. Mekata, H. Kuriyama, Y. Ajiro, S. Mitsuda, and H. Yoshizawa, J. Magn. Magn. Mater. **104–107**, 859 (1992).
[35]H. Schmid, J. Phys.: Condens. Matter **20**, 234201 (2008).
[36]J. W. Cable, M. K. Wilkinson, E. O. Wollan, and W. C. Koehler, Phys. Rev. **125**, 1860 (1962).
[37]T. Sato, H. Kadowaki, and K. Iio, Physica B: Condensed Matter **213-214**, 224 (1995).
[38]S. Seki, H. Murakawa, Y. Onose, and Y. Tokura, Phys. Rev. Lett. **103**, 237601 (2009).